Nanoscale topography templates the organization of stable clathrin/AP-2 structures

T. Sansen[1, ±], D. Sanchez-Fuentes[2, ±], R. Rathar[1, ±], A. Colom-Diego[3], F. El Alaoui[1], S. de Rossi[4], J. Viaud[5], M. Macchione[6], S. Matile[6], R. Gaudin[1], A. Carretero-Genevrier[2,*], and L. Picas[1,*]

[1]Institut de Recherche en Infectiologie de Montpellier (IRIM). CNRS UMR 9004 – Université de Montpellier, Montpellier, France.

[2]Institut d'Électronique et des Systèmes (IES), CNRS UMR 5214 – Université de Montpellier, Montpellier, France.

[3]Biochemistry Department and School of Chemistry and Biochemistry, University of Geneva, Geneva, Switzerland. Swiss National Centre for Competence in Research Program. Swiss National Centre for Competence in Research Programme Chemical Biology, Geneva, Switzerland.

[4]MRI, Imaging facility, UMS BioCampus Montpellier, France.

[5]Inserm U1048 and Université Toulouse 3, I2MC, Avenue Jean Poulhès BP84225, 31432 Toulouse Cedex 04, France.

[6]School of Chemistry and Biochemistry, University of Geneva, Geneva, Switzerland. Swiss National Centre for Competence in Research Program. Swiss National Centre for Competence in Research Programme Chemical Biology, Geneva, Switzerland.

[±]Equal contribution

*Correspondence sent to: carretero@ies.univ-montp2.fr; laura.picas@irim.cnrs.fr

Eukaryotic cells are constantly submitted to shape changes as a result of fundamental cellular processes such as cell differentiation, migration or division, but also as a response to the extracellular environment. Previous studies point out to the plasma membrane

curvature as a major mechanosensing mechanism[1,2], although other processes might participate in the biochemical transduction of topographical cues[3]. Thus, how cells sense and respond to the external topography is not well understood. A bottleneck to address this question demands to conciliate the time-consuming and limited access to top-down nanofabrication techniques with cell biology and advance microscopy approaches. Here, we have engineered 1D SiO_2 nanopillar arrays of defined sizes and shapes on high-performance coverslips by soft-gel nanoimprint lithography (soft-NIL)[4], which is a cost-effective, customizable, large-scale fabrication and benchtop equipment-based method. By this novel fabrication of nanostructured substrates, we were able to perform super-resolution microscopy and to demonstrate that large membrane morphologies favor the formation of stable clathrin/AP-2 structures, a process that is assisted by the formation of functional actin networks.

The key interface mediating the first interaction of cells with the extracellular matrix is the plasma membrane. The ability of the plasma membrane to reshape in response to external mechanical stimuli and to trigger biochemical signals through the recruitment and/or disassembly of membrane-associated proteins is a fundamental feature to preserve cellular hemostasis[3]. Thus, the plasma membrane is no longer considered as a passive barrier but as a mechanosensing structure connecting the cell with its environment. A powerful approach to investigate the response of living cells to topography changes of the external milieu consist on the engineering of vertical nanostructures such as nanopillars[1], nanoneedles[5] or nanocones[2], among others, primary obtained by top-down procedures, such as focused ion beam (FIB). By using these devices, it was shown that topography-induced curvature is able to modulate cellular processes such as membrane trafficking[1], cytoskeleton organization[6] and nuclear mechanotransduction[6]. Indeed, the recruitment of curvature-sensing proteins implicated in the formation of "canonical" clathrin-coated structures was shown to be enhanced by seeding living cells on nanostructures with a curvature diameter below 400 nm[1,2]. However, endocytic proteins

such as clathrin or dynamin have been reported to be localized on larger membrane structures that are typically associated to the actin cytoskeleton, such as membrane protrusions at sites of cell-cell fusion[7] or on microvillus-related structures of polarized MDCK cells[8], among other examples[8]. Indeed, the actin cytoskeleton is implicated in the force-generation and remodeling of membranes during cell morphological changes, as a result of the attachment of the actin cytoskeleton with the plasma membrane at the cell cortex and the regulation of the cortical tension[9].

To investigate how actin organization and the localization of endocytic proteins is affected by the shape of large membrane structures, we engineered arrays of 1D SiO_2 nanopillars of defined dimensions (*D*) and shape: *D* ~ 400 nm (circular shape), *D* ~ 600 nm (circular shape), D ~ 850 nm (square shape), as determined from scanning electron microscopy (SEM) and Atomic Force Microscopy (AFM) (see Supplementary Fig. 1 and Supplementary Table 1). Briefly, we customized soft Nano-Imprint Lithography (NIL) of epitaxial α-quartz (SiO_2) thin films[10,11] by combining top-down and bottom-up (sol-gel) approaches to fabricate nanostructured SiO_2 layers of controlled shape, diameter and periodicity on high-performance coverslips made of borosilicate glass, which are the substrate of choice for super-resolution microscopy applications[12]. Our experimental process included the combination of dip-coating method to synthetize sol-gel silica films of controlled thicknesses on borosilicate glass coverslips with Laser Interference Lithography (LIL)[13] and NIL lithographic techniques. In a first top-down fabrication step, extensive Si(100) masters made of nanopillars arrays were obtained by using LIL and transferred by reactive ion etching at low pressure (see details in the methods section). Then, a second step involved the preparation of high quality PolyDiMethylSiloxane (PDMS) molds from Si(100) masters (Supplementary Fig. 2) that produce perfectly imprinted silica nano-pillars with controlled diameter and height on silicon, as illustrated in Fig. 1 and Supplementary Fig. 1 and 3.

We confirmed that our substrates induce controlled plasma membrane deformations by seeding HeLa cells on vertical SiO_2 nanocolumns coated with poly-L-lysine, as revealed from

fluorescence microscopy images using cell plasma membrane markers, such as the mCherry-MyrPalm (Fig. 1 and Supplementary Fig. 4). Membrane shape induced by vertical nanopillars was also confirmed by Scanning Electron Microscopy (SEM), as shown in Fig.1. Altogether these results confirm that soft-NIL engineered vertical SiO_2 nanopillar's arrays are suitable setups to exert controlled plasma membrane deformations on adherent cells.

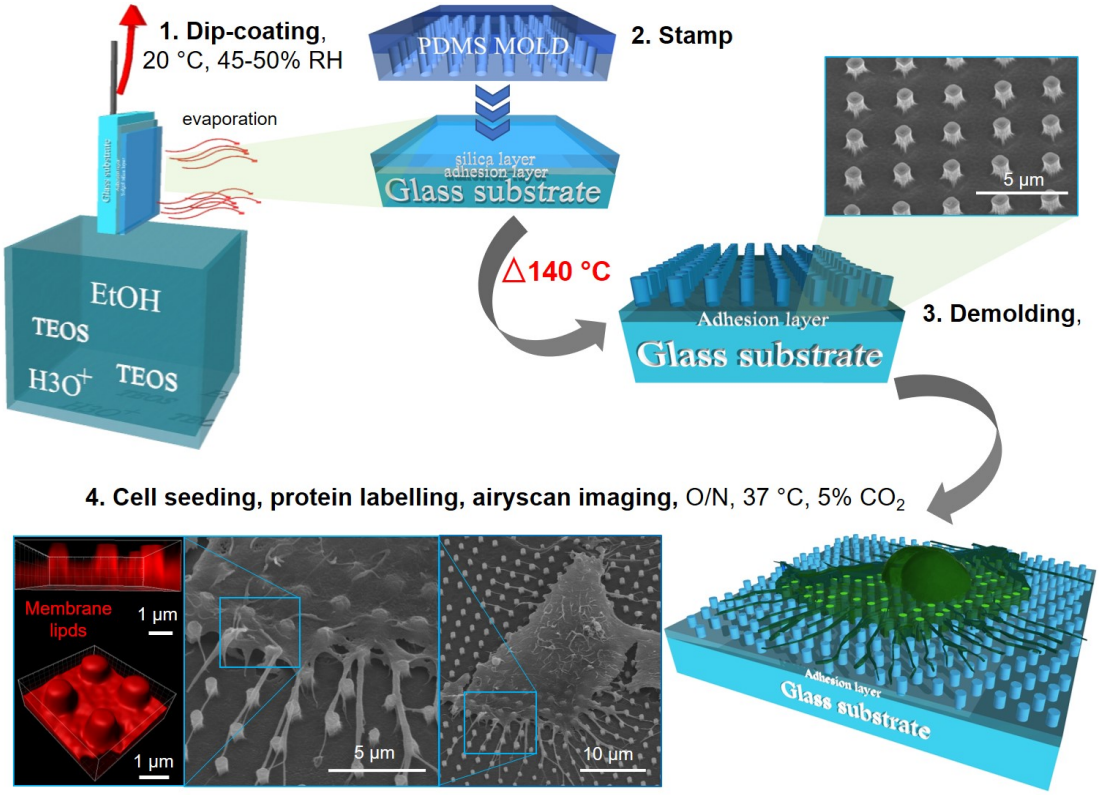

Figure 1. Schematic representation of the nanostructuration of SiO_2 substrates by soft Nano-Imprint Lithography to modulate the shape of cellular membranes. The main steps in the fabrication of 1D vertical SiO_2 nanopillar arrays consisted in 1) dip-coating of a thin SiO_2 sol-gel layer on high-performance coverslips, 2) stamping of the sol-gel layer with a PDMS mold, previously generated by LIL, 3) consolidation of the SiO_2 sol-gel layer at high temperature (140°C) to create solid 1D vertical SiO_2 nanostructures, as revealed by the SEM image. 4) Seeding of adherent cells on nanostructured SiO_2 substrates allows to exert nanopillar-induced membrane deformations, as visualized by either SEM (*right and central panel*) or fluorescence microscopy of cell membrane lipids (*red, left panel*).

We have applied our vertical SiO_2 nanopillars to monitor changes in the organization of the actin cytoskeleton in response to external topographical cues, by seeding HeLa cells on arrays of 1D nanopillar's with a 1:1 aspect ratio and the three dimensions, *D*, aforementioned. Cells

were then stained with phalloidin and imaged by Airyscan, a recently developed 2D single-point scanning super-resolution mode that improves by 1.7-fold the lateral resolution and ~5-fold the volumetric resolution of conventional confocal microscopy[12]. Z-projection images of the entire pillar's length in Fig. 2a show that the actin cytoskeleton is organized around 1D nanopillars but not enriched with respect to other regions of the cell (away from pillars), as revealed by a median enrichment index (E, see the methods section) of $E \sim 1$ for any of the dimensions tested in this study and displayed in Fig. 2b. The 3D reconstruction of HeLa cells seeded on nanopillars arrays of $D \sim 600$ nm (circular shape) and co-immunostained against key endocytic proteins such as clathrin and AP-2[14] and the membrane lipid phosphatidylinositol 4,5-bisphosphate ($PI(4,5)P_2$)[15] displayed in Fig. 2c shows a distinct 3D localization of the four cellular markers. $PI(4,5)P_2$ is found all over the membrane that wraps up the nanopillar structure, whereas actin, clathrin and AP-2 preferentially localize at the base of nanopillar, although clathrin is also organized all along the pillar's length. The profile analysis of the actin, clathrin, and AP-2 signals suggests that the three proteins are predominantly associated around the nanopillars (Fig. 2d). To confirm that the organization of actin, clathrin and AP-2 at the cell membrane is well imposed by the topography of substrate, we analyzed the 2D autocorrelation of the three fluorescent signals on HeLa cells seeded on 1D nanopillar's displaying two different shapes: circular shape ($D \sim 400$ nm) and square shape ($D \sim 850$ nm), as shown in Fig 2e and f, respectively. We obtained a periodic distribution of 1086 ± 70 nm, 1047 ± 50 nm, and 1041 ± 60 nm for cells seeded on pillars of $D \sim 400$ nm, and 2409 ± 4 nm, 2374 ± 10 nm and 2405 ± 20 nm (mean ± s.d., $N \geq 5$) for cells seeded on pillars of $D \sim 850$ nm, for actin, AP-2 and clathrin, respectively (arrowheads, Fig. 2e-f), in agreement with the distribution of the engineered SiO_2 nanopillar's arrays (Supplementary table 1). Moreover, we found a long-range patterning for either actin, AP-2 and clathrin signals, suggesting that the transduction of topographical cues by the cell is not a discrete process. The distribution of the autocorrelation amplitude was of ~20% for all the three proteins on the circular shape pillar and shifted to lower values for AP-2 as compared to the ~25% amplitude obtained for actin and

clathrin on the square nanopillars. High magnification of long-range 2D periodic lattices showed ring-like isotropic organization of actin around nanopillars irrespective of the pillar's shape, whereas clathrin and AP-2 display an isotropic organization on circular shape pillars and anisotropic in the case of square shape nanopillars (insets, Fig. 2e and f). The different behaviors observed might reflect the distinct nature of membrane association of these proteins and the different supra-molecular organization, as a result of their intrinsic ability to form semi-flexible polymers, such as actin[16], or to oligomerize into a lattice-like structures, as in the case of clathrin[17]. Collectively, these results indicate a topography-mediated organization of clathrin and AP-2 at the plasma membrane that is associated to the presence of the actin cytoskeleton around the nanopillar's base.

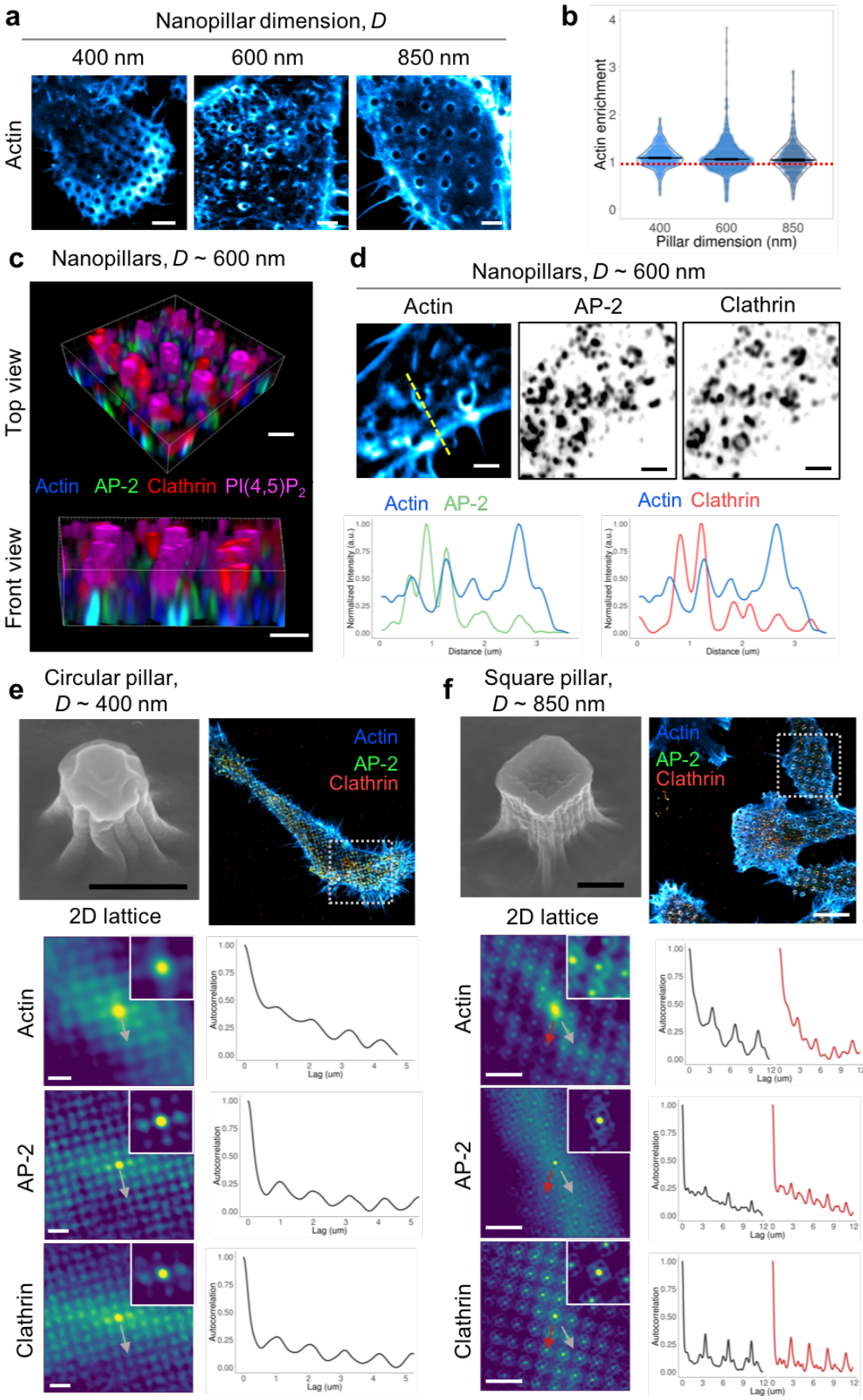
a
Nanopillar dimension, D
400 nm
600 nm
850 nm
Actin
b
Actin enrichment
Pillar dimension (nm)
c
Nanopillars, D ~ 600 nm
Top view
Front view
Actin AP-2 Clathrin PI(4,5)P2
d
Nanopillars, D ~ 600 nm
Actin
AP-2
Clathrin
Actin AP-2
Actin Clathrin
Normalized Intensity (a.u.)
Distance (um)
e
Circular pillar, D ~ 400 nm
Actin
AP-2
Clathrin
2D lattice
Autocorrelation
Lag (um)
f
Square pillar, D ~ 850 nm
Actin
AP-2
Clathrin
2D lattice
Autocorrelation
Lag (um)

Figure 2. 1D nanopillar's arrays template the localization of actin, clathrin and AP-2 at the plasma membrane. a, Staining of F-actin on HeLa cells seeded on arrays of vertical SiO_2 nanopillars of dimensions $D \sim$ 400 nm, $D \sim$ 600 nm, and $D \sim$ 850 nm. Images are maximum intensity projections of z-stacks. Scale bar, 2 μm. **b,** Enrichment, E, of F-actin on HeLa cells seeded on nanopillars of different dimensions. The number of data points per condition is: n=756, n=1183, n=649, for $D \sim$ 400 nm, $D \sim$ 600 nm, and $D \sim$ 850 nm, respectively. Dotted red line indicates an $E \sim 1$. **c,** 3D reconstruction of a top view and cross-section of HeLa cells seeded on nanopillars of $D \sim$ 600 nm and immunostained for actin (*blue*), AP-2 (*green*), clathrin (*red*), and PI(4,5)P_2 (*magenta*). Scale bar, 1 μm. **d,** High-magnification of maximum intensity projection of z-stacks from HeLa cells seeded on nanopillars of $D \sim$ 600 nm and immunostained for actin (*blue*), AP-2 (*green*), and clathrin (*red*). Profile analysis along the dotted yellow line in the corresponding image. Scale bar, 1 μm. **e,** *Left,* High-magnification SEM image of a circular nanopillar of $D \sim$ 400 nm. Scale bar, 400 nm. *Right,* maximum intensity projection of an airyscan image of HeLa cells seeded on circular nanopillars, $D \sim$ 400 nm, immunostained for actin (*blue*), AP-2 (*green*), and clathrin (*red*). Scale bar, 10 μm. *Bottom*, 2D autocorrelation function of actin, AP-2, and clathrin signals corresponding to the white dashed box. Insets, 4X magnifications of the corresponding 2D-lattice. Scale bar, 2 μm. 1D autocorrelation function, as indicated by the gray arrowhead in the corresponding image. **f,** same as e, but on rectangular nanopillars of $D \sim$ 850 nm. Two directions in the 1D autocorrelation function are displayed by a gray and red arrowheads on the corresponding image.

Next, we assessed if the range of membrane shapes selected in this study and imposed by the underlying 1D nanopillar's arrays where the cells are seeded might enhance the accumulation of endocytic proteins, for instance as previously reported by *in cellulo* studies during cell-cell fusion[7]. The immunostaining of AP-2 and clathrin on HeLa cells seeded on vertical nanopillars of $D \sim$ 400 nm, $D \sim$ 600 nm and, $D \sim$ 850 nm revealed that both proteins preferentially accumulate at the plasma membrane-nanopillar interface compared to regions of the cell membrane that are adhered to the flat substrate (not on pillars), as shown in Fig. 3a-b. Indeed, we estimated in all cases a median value of $E \geq 2$, which was steady at E~2.5 for AP-2, irrespective of the nanopillar's dimensions, and $2 \leq E \leq 3.5$ in the case of clathrin. This behavior was specific of clathrin-associated proteins, as revealed by a preferential enrichment of the endocytic protein caveolin-1[18] on nanopillar's arrays of $D \sim$ 600 nm with an $E \sim 4$ but not on other pillar's dimensions ($E \leq 1.5$) (Supplementary Fig. 5). Conversely, the GTPase dynamin-

2, which is downstream the clathrin-coat assembly and formation[14], displayed a moderate but steady enrichment of $1.5 \leq E \leq 2$ (Supplementary Fig. 6), which recalls the same trend observed for clathrin and AP-2. This behavior agrees with the fact that dynamin-2 was also localized together with clathrin in large membranes protrusion during osteoclast cell-cell fusion[7]. Finally, the epidermal growth factor receptor (EGFR), which is a clathrin-internalized cargo responsible for gene expression regulation[19], showed a size-dependent enrichment with a preferential accumulation of the receptor for nanopillars of $D \sim 400$ nm ($E \sim 2.5$) but not for dimensions $D \geq 600$ nm ($E \sim 1$) (Supplementary Fig. 7). This observation is consistent with the strong preference of endocytic "canonical" clathrin-coated structures for positive curvatures with a diameter < 400 nm. A possible explanation for the steady accumulation of clathrin and AP-2 at the plasma membrane-pillar interphase, irrespective of the pillar's dimensions, might rely on the local membrane lipid composition. Indeed, plasma membrane phosphoinositides (PIs) are key regulators of the clathrin-coat assembly and maturation during endocytosis[15] and are implicated in actin polymerization[20]. The endogenous localization of the main PIs present at the plasma membrane - PI(4,5)P_2 and PI(3,4,5)P_3- of HeLa cells seeded on vertical nanopillars of different dimensions was revealed by immunostaining using fluorescent recombinant PI-binding motifs[21] and showed an absence of significant enrichment of PIs due to the pillar's topographical stimuli with an $E \leq 1.5$ (Supplementary Fig. 8a-b). Thus, the steady accumulation of clathrin and AP-2 due to topography features is not likely to rely on the local segregation of PIs, although we could not exclude that a moderate but local fold increase of $1 \leq E \leq 1.5$ might be enough to trigger an acute PI-mediated response and thus, future experiments should be conducted in this direction.

The consistent organization of actin around vertical nanopillars irrespective of their dimensions and the linear correlation that we found between the enrichment of clathrin and AP-2 with the presence of F-actin (Fig. 3c), led us wonder if the sustained accumulation of endocytic proteins might be an actin-mediated process. To test this hypothesis, we subjected HeLa cells previously seeded on nanopillar's arrays of $D \sim 600$ nm to two actin modulating drugs: Cytochalasin D

(CytoD), which inhibits actin polymerization, and jasplakinolide (Jasplak), which stabilizes actin microfilaments and prevents actin depolymerization, as shown in Fig. 3d. We found that CytoD treatment did lead to an absence of difference in the accumulation of clathrin and AP-2 on pillars, possibly as a result of the formation of actin patches around nanopillars that we observed on cells treated with this drug. This was not the case of cells treated with jasplakinolide, which showed a 2-fold increase in the median enrichment value, *E*, for both AP-2 and clathrin. These results suggest that the accumulation of AP-2 and clathrin in response to a topographical stimulus would rely on the formation of actin networks, typically occurring at the base of vertical nanopillars (Fig. 2 and Fig. 3e).

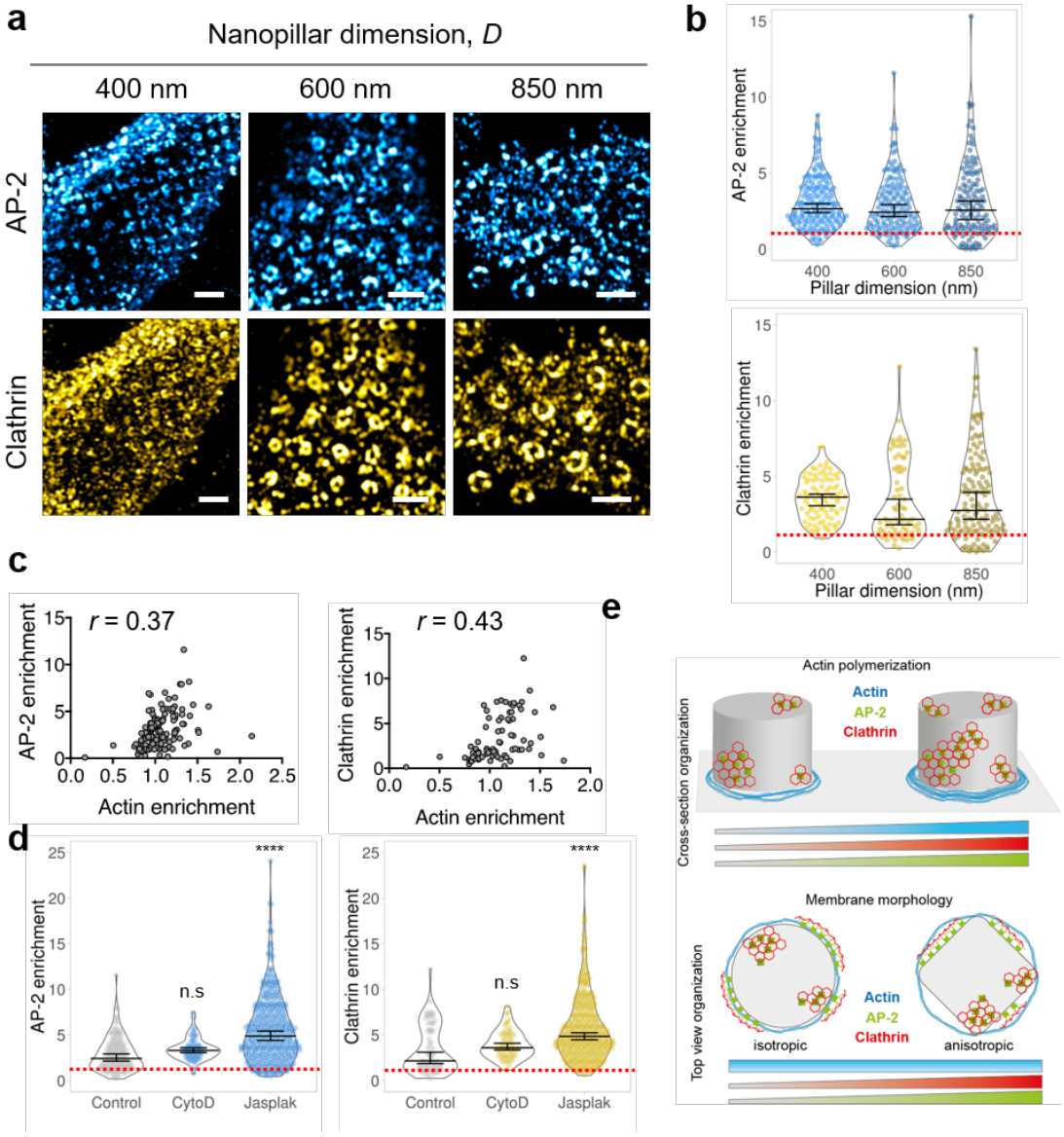

Figure 3. The formation of actin networks enhance the accumulation of clathrin and AP-2 at the plasma membrane-nanopillar interface. a, Immunostaining of AP-2 (*blue*) and clathrin (*gold*) on HeLa cells seeded on nanopillars of dimensions $D \sim 400$ nm, $D \sim 600$ nm, and $D \sim 850$ nm. Images represent maximum intensity projections of z-stacks. Scale bar, 2 μm. **b,** Enrichment, E, of AP-2 (*blue*) and clathrin (*gold*) from immunostained HeLa cells seeded on nanopillars of different dimensions. The number of data points per condition is n=171, n=146, n=133 and for for AP-2 and n=89, n=75, n=132 for clathrin, for the nanopillar's $D \sim 400$ nm, $D \sim 600$ nm, and $D \sim 850$ nm, respectively. Dotted red line indicates an $E \sim 1$. **c,** Scatter plots showing the correlation between the enrichment of actin and AP-2 (*left*) or clathrin (*right*) on HeLa cells seeded on nanopillars of $D \sim 600$ nm. The correlation coefficient (r) is indicated. **d,** Enrichment, E, of AP-2 (*blue*) and clathrin (*gold*) from immunostained HeLa cells seeded on nanopillars of $D \sim 600$ nm after treatment with CytochalasinD (CytoD) or Jasplakinolide (Jasplak). The non-treated condition is shown in grey. The number of data points per condition is n=146, n=62, n=429 for AP-2 and is n=75, n=62, n=430 for clathrin, for the non-treated, CytoD, and Jasplak condition, respectively. Dotted red line indicates an $E \sim 1$. **e,** Schematics of the effect of actin polymerization (*top*) and membrane morphology (*bottom*) in the localization of actin (*blue*), AP-2 (*green*) and clathrin (*red*) on nanopillars inducing large plasma membrane deformations > 400 nm.

The strong coupling of the plasma membrane to the underlying actin cortex is an essential regulator of the mechanical state of the cell membrane[9]. As a result, we reasoned that the remodeling of the actin cytoskeleton that we observed in response to the topography of 1D vertical nanopillars might be transduced by a change in the plasma membrane tension. We estimated the tension of the plasma membrane-pillar interface of HeLa cells seeded on 1D vertical nanopillars by using the fluorescent membrane tension sensor FliptR, which provides a direct estimation of the membrane tension of living cells by using fluorescence lifetime imaging microscopy (FLIM), as previously reported[22]. The resulting mean FliptR lifetime showed that plasma membrane tension increases by decreasing the nanopillar's dimension, i.e. $\tau = 4.19 \pm 0.34$, $\tau = 4.05 \pm 0.38$ $\tau = 3.97 \pm 0.19$ (mean ± s.d.), for $D \sim 400$ nm, $D \sim 600$ nm, $D \sim 850$ nm, respectively (Fig. 4a-b), therefore suggesting that for an equivalent projected area the force generated by the actin network organization around nanopillars of different dimensions and transmitted to the cell cortex should have a different contribution on the apparent plasma membrane tension. However, increase in plasma membrane tension caused by

osmotic swelling (Π < 300 mOsm)[23] of HeLa cells seeded on vertical nanopillars of $D \sim 850$ nm showed a moderate 1.2-fold increase in the enrichment of AP-2 on pillars but had no effect on clathrin and actin localization (Fig. 4c and Supplementary Fig. 9). This observation suggests that on large membrane deformations induced by vertical nanostructures the membrane-association of clathrin and AP-2 would be dominated by the force generated by functional actin networks over the contractility-independent mechanotransduction that was previously reported for clathrin-coated structures[24], at least under relatively high substrate rigidly conditions. Next, we wonder whether different modes of dynamics might be associated to the clathrin and AP-2 structures present on nanopillars compared to conventional flat glass substrates. Spinning disk confocal analysis of genome edited SUM-159 cells expressing the σ2 subunit of the AP-2 complex fused to EGFP showed a homogenous distribution of AP-2 along the basal cell membrane of cells seeded on conventional glass substrates compared to the accumulation of stable AP-2 at the membrane-pillar interface (Fig. 4d). Moreover, AP-2 structures associated to nanopillars display a 1.5-fold increase in both the maximum intensity and mean lifetime as well as the appearance of a population of structures shifted towards longer lifetimes to those expected for "canonical" coated pits, i.e. > 60 s[25], as compared to flat substrates. Collectively, these results suggest that topographical cues imposed by the large vertical nanostructures, $D >$ 400 nm, drive the formation of stable clathrin/AP-2 structures, with a similar dynamic to that reported for long-lived and large clathrin lattices[25].

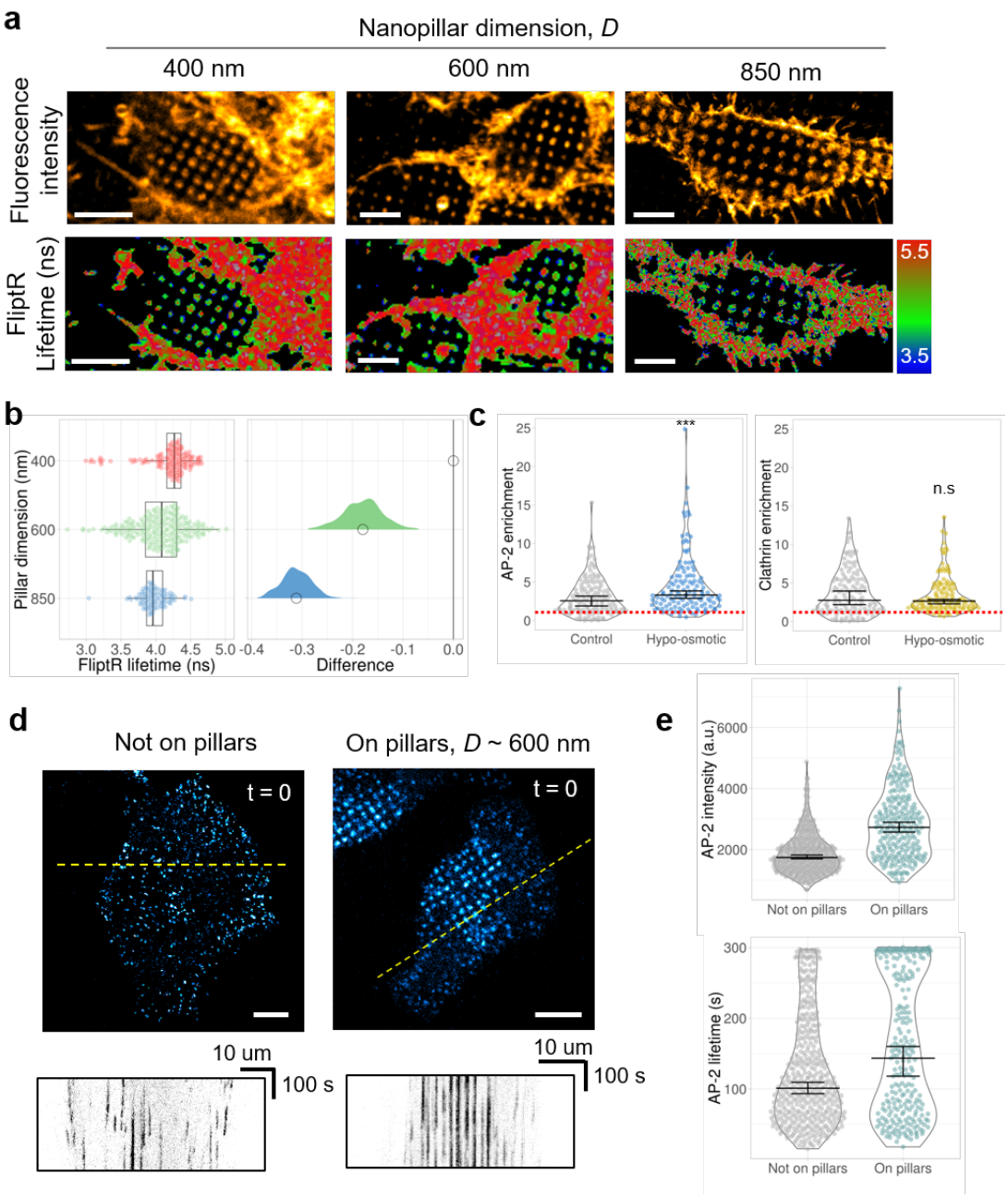

Figure 4. Vertical nanopillars modulate the plasma membrane tension and the formation of stable AP-2/clathrin-coated structures. a, Confocal (*upper*) and FLIM (*lower*) images of the plasma membrane of HeLa cells seeded on vertical nanopillars of $D \sim 400$ nm, $D \sim 600$ nm, and $D \sim 850$ nm and stained with the membrane tension probe FliptR. The color bar code corresponds to lifetime in ns. Scale bar, 2 µm. **b, c,** Enrichment, E, of AP-2 (*blue*) and clathrin (*gold*) from immunostained HeLa cells seeded on nanopillars of $D \sim 850$ nm under hypo-osmotic shock ($\Pi < 300$ mOsm). Comparison with the isotonic condition is shown in grey. The number of data points per condition is n=133, n=128 for AP-2 and is n=132, n=129 for clathrin, for the isotonic and hypo-osmotic condition, respectively. Dotted red line indicates an $E \sim 1$. **d,** The dynamics of clathrin-coated structures was obtained by spinning disk microscopy every 2s for 5 min on genome edited AP-2 σ2-EGFP SUM159 cells seeded

on either conventional SiO_2 coverslips (*not on pillars*) or on coverslips with nanopillars of $D \sim 600$ nm. Images represent maximum intensity projections of z-stacks. Kymographs were performed along the dotted yellow line shown in the corresponding image in **d**. **e,** Quantification of the AP-2 maximum intensity (in a.u.) and lifetime (in s) of clathrin-coated structures on genome edited AP-2 σ2-EGFP SUM159 cells seeded on nanopillars of $D \sim 600$ nm (*cadetblue*) and on conventional SiO_2 coverslips (*in gray*), as observed in the kymographs in **b**. The number of data points per condition is n=440 and n=255 for cells seeded not on pillars and on pillars, respectively.

In conclusion our work shows the potential of a straight-forward and cost-effective nanostructuration method based on soft-NIL to engineer well-defined arrays of vertical nanostructures to investigate the effect of sustained external topographical cues on the mechanochemical response of the cell plasma membrane. This novel strategy of high-performance glass nanostructuration combined to super-resolution microscopy technique has provided unprecedented insight on the mechanistic behind the topography-driven organization of the actin cytoskeleton and a subset of endocytic proteins. Our results show that the membrane morphology imposed by the topography of vertical nanostructures larger than 400 nm templates the organization of stable clathrin/AP-2 structures, a process that is assisted by the force-generated and remodeling of functional actin networks at the base of nanopillars. Therefore, cells might engage a morphology-dependent response to the topographical features of the external environment: by privileging a curvature-sensing response and the formation of clathrin-coated hotspots at diameters < 400 nm[1,2] or a local force-sensing response with the formation of stable clathrin-coated structures at larger membrane shapes, > 400 nm, as we showed in this study.

Methods

Synthesis of silica sol-gel thin films

Solution preparation: All the chemicals were from Sigma-Aldrich and without any further purification. Silica precursor solution were prepared by adding 4.22 g tetraethyl orthosilicate

(TEOS) into 23.26 g absolute ethanol, then 1.5 g HCl (37%), and stirring the solution for 18 h. The final molar composition was TEOS:HCl:EtOH=1:0.7:25.

Gel films by dip-coating: layer gel films on high-performance coverslips made of borosilicate glass of the first hydrolytic class with precision thickness No. 1.5 (0.170 ± 0.005 mm) at room temperature were prepared with a ND-DC300 dip-coater (Nadetech Innovations) equipped with an EBC10 Miniclima Device to control the surrounding temperature and relative humidity. During the dip-coating, we fixed the ambient temperature and relative humidity as 20ºC and 45-50% and the thickness of film was controlled by the withdrawal rate. In this study, all the films were made at withdrawal rate of 300 mm/min i.e. 200 nm thick to ensure the nanoimprint process. After dip-coating, as-prepared gel films were consolidated with a thermal treatment of 5 min at 430 ºC under air atmosphere.

Silica thin film nanostructuration

Molds preparation: Si masters were elaborated using LIL Lithography as previously reported[10,11]. Briefly, this procedure allows to quickly obtain periodic patterns on silicon substrates of controlled shape (square and circular, as previously described[26], diameter and periodicity over a large surface (~cm^2) without the need of a lithographic mask[13].

PDMS (polydimethylsiloxane) reactants (90 w% RTV141A; 10 w% RTV141B from BLUESIL) were transferred onto the master and dried at 70 °C for 1 h before unmolding.

Then, a first silica layer seed was deposited at a constant relative humidity of 45-50% at 20ºC with controlled withdrawal speeds of 300 mm min^{-1} in order to adjust the final thickness to 200 nm, and was consolidated at 430ºC for 5 min. Importantly, this film has an important functionality as an adhesion layer to faultlessly replicate the columnar shape from the PDMS mold. Then, a new layer of the same solution was deposited under the same conditions for printing. Imprinting of sol–gel films with a PDMS mold involves the following steps. First, molds were degassed under vacuum (10 mbar) for 20 min before direct application on the as-prepared xerogel films kept in a controlled environment, without additional pressure. After

imprinting, the samples were transferred to a 70 °C stove for 1 min and then to a 140 °C stove for 2 min to consolidate the xerogel films before peeling off the PDMS mold. Next, the sol–gel replicas were annealed at 430 °C for 10 min for consolidation. Notice that, a new multiple replication process to reduce the dimensions of silica nanopillars in a controlled manner has been developed. This method consisted of producing PDMS molds from each sol-gel replica successively as illustrated in supplementary figure 3, then the silica nanopillar reduces their dimension of 40% each NIL process which correspond around 200 nm less in height from the original silicon master, after consolidation at 430 °C during 10 min.

Structural Characterization of nanostructured silica pillars

The microstructures of the films were investigated with a FEG-SEM model Su-70 Hitachi, equipped with an EDX detector X-max 50 mm^2 from Oxford instruments. Atomic Force Microscopy (AFM): The topography of quartz films was studied by tapping Atomic Force Microscopy (AFM) images obtained using Park Systems NX-10 Scanning Probe Microscopy (SPM) unit.

Cell lines and constructs

HeLa cells (a gift from B. Goud, Institut Curie, CNRS UMR 144, Paris, France) were cultured in DMEM GlutaMAX supplemented with 10% fetal calf serum and 100 $U{\cdot}mL^{-1}$ of penicillin and streptomycin at 37ºC in 5%CO_2. Genome edited SUM-159 AP2 σ2-EGFP +/+ cells and SUM-159 Dynamin2-EGFP +/+ AP2 σ2-TagRFP-T +/+ previously described[27,28] and cultured in DMEM/F12 (1:1) GlutaMAX supplemented with 5% fetal calf serum, 100 $U{\cdot}mL^{-1}$ of penicillin and streptomycin, 1$\mu g{\cdot}mL^{-1}$ Hydrocortisone, 5$\mu g{\cdot}mL^{-1}$ insulin and 10mM HEPES at 37ºC in 5%CO_2. All cell lines were tested for mycoplasma.

mCherry-MyrPalm was a gift from Gaelle Boncompain, Insitut Curie, CNRS UMR 144, Paris, France). EGFR-GFP was a gift from Alexander Sorkin (Addgene plasmid #32751). Plasmids were transfected 24h after cell seeding using JetPEI® transfection reagent (Polyplus transfection®) according to the manufacturer's instructions.

Antibodies and drugs

Mouse monoclonal anti-adaptin α (Cat. Nr. 610501) was obtained from BD Transduction Laboratories (Becton Dickinson France SAS, France). Polyclonal rabbit anti-clathrin heavy chain (CLTA - Cat. Nr. SAB1410212) was from Sigma. Rabbit monoclonal anti-caveolin-1 (Cat. Nr. SC-53564) was from Santa Cruz Biotechnology, Inc. Phalloidin-Atto 390 (Cat. Nr. 50556) was obtained from Sigma. Secondary antibodies were from Jackson ImmunoResearch Laboratories Inc.: Donkey anti-Mouse IgG (H+L) conjugated to Cy3 (Cat. Nr. 715-165-150) and Alexa Fluor® 488 (Cat. Nr. 715-545-150). Donkey anti-Rabbit IgG (H+L) conjugated to Cy3 (Cat. Nr. 715-165-152). Cytochalasin D (Cat. Nr. C8273), Jasplakinolide (Cat. Nr. J4580) and Poly-L-lysine (Cat. Nr. P4707) were purchased from Sigma-Aldrich. Actin disturbing drugs were added to seeded cells at the following final concentrations: Cytochalasin D at 5μg. mL^{-1} and Jasplakinolide at 1μM for 15 min at room temperature before fixation, as described in[29]. Hypo-osmotic shock was performed for 5 min before fixation as described in[29].

Phosphoinositide's probes

Recombinant GST-tagged PH-domain of PLCδ detecting the membrane lipid $PI(4,5)P_2$ was produced and conjugated to of amine-reactive Alexa Fluor 647 carboxylic acid succinimidylester (Invitrogen) as previously described[30]. Recombinant eGFP-GST-tagged PH-domain of Grp1 detecting the membrane lipid $PI(3,4,5)P_3$ was expressed overnight at 18 ºC using 1 mM IPTG in Escherichia coli strain BL21(DE3) and purified by affinity chromatography using glutathione Sepharose 4B beads according to the manufacturer's instructions (GE Healthcare) in 50mM Tris at pH 8.0, 100mM NaCl. Finally, the motif was dialyzed overnight in a Slide-A-Lyzer dialysis cassette (MWCO 10,000) and the concentration was measured using a Bradford assay (Biorad).

Immunofluorescence

Cells seeded on SiO_2 nanostructured substrates were fixed and permeabilized in 3.7% PFA, 0.05% Triton X-100 in PBS for 20 min at room temperature, then rinsed in PBS twice and incubated for 30 min at room temperature in 1% BSA. Coverslips were then stained for the primary antibodies for 45 min. Then, secondary antibodies were incubated for 45 min. Phalloidin and PI-probes were also incubated for 45 min at a final concentration of 0.4µM and 40 µg. mL^{-1}, respectively. Finally, coverslips were soaked in PBS, then in sterile water and mounted with a Mowiol® 4-88 mounting medium (Polysciences, Inc.). Montage was allowed to solidify in the dark for 48h before microscope acquisitions.

Airyscan microscopy

Images were acquired on a Zeiss LSM880 Airyscan confocal microscope (MRI facility, Montpellier). Excitations sources used were: 405 nm diode laser, an Argon laser for 488 nm and 514 nm and a Helium/Neon laser for 633 nm. Acquisitions were performed on a 63x/1.4 objective. Multidimensional acquisitions were acquired via an Airyscan detector (32-channel GaAsP photomultiplier tube (PMT) array detector). 3D images were acquired by fixing a 0.15µm z-step to generate a z-stack of images (z-stack ~ 10) that cover the entire nanopillars length.

Spinning disk microscopy of living cells

Live cell imaging of genome edited SUM-159 AP2-σ2-EGFP cells seeded on arrays of 1D nanopillars with $D \sim 600$ nm was performed using a spinning disk confocal microscopy (Nikon TI Andor CSU-X1 equipped with a Yokogawa spinning disk unit (Andor)) (MRI facility, Montpellier) equipped with a 488 laser beam (60 mW). Acquisitions were performed with a 60x/1.4 objective. During imaging, cells were maintained at 37°C, 5%CO_2 in an onstage incubator (Okolab). Movies were recorded with a mono dichroic mirror (488nm) and a GFP emission filter (525-30nm). Samples were exposed to laser light for 100ms every 2s for 5 min

and images were acquired using an EMCCD iXon897 (Andor) camera. A 0.15µm z-step was used to cover all the nanopillars length in every z-stack acquisition.

Fluorescence lifetime imaging microscopy of live cells

FLIM measurement of FliptR lifetime on living cells were performed as previously reported[22]. Briefly , Hela cells were seeded on nanostructured SiO_2 structures overnight as stated above. Then, the culture medium was replaced with the same medium containing 1.5 μM of the FliptR probe and incubated for 10 min. FLIM imaging was performed using a Nikon Eclipse Ti A1R microscope equipped with a Time Correlated Single-Photon Counting module from PicoQuant. Excitation was performed using a pulsed 485nm laser (PicoQuant, LDH-D-C-485) operating at 20 MHz, and emission signal was collected through a bandpass 600/50 nm filter using a gated PMA hybrid detector and a TimeHarp 260 PICO board (PicoQuant). SymPhoTime 64 software (PicoQuant) was then used to fit the fluorescence decay data (from either full images or regions of interest) to a dual exponential model after deconvolution for the instrument response function.

Data analysis and processing

The preferential localization of each cellular component of interest at the plasma membrane interface with the vertical nanopillars was determined by estimating an enrichment (E), as detailed as follows,

$$E = (I_p/I_f)_{SOI}/(I_p/I_f)_{membrane},$$

which reports the ratio between a signal of interest (SOI), at the plasma membrane bent by the pillars (Ip) versus the SOI at the flat membrane surface (If, not on pillar). This ratio was then normalized by an unspecific plasma membrane marker (e.g. mCherry-MyrPalm) on pillars and not on pillars to correct for topographical artifacts on our estimations. We considered that an $E > 1$ reports that the SOI has a preference for the plasma membrane that is at the interface with the nanopillar. Thus, the higher the E, the larger the tendency of a SOI to be localized on

nanopillars. Conversely, an E of 1 or below would indicate that there is no preferential localization of a SOI for either the membrane that is bent over the pillar or the plasma membrane that is adhered on the flat substrate.

The enrichment (*E*) was obtained from maximum intensity projection of z-stack images acquired by Airyscan imaging. Each acquisition was treated by using a semi-automatic detection of each SOI on pillars and not on pillars using built-in macro functions and the ImageJ software[31].

2D autocorrelation analysis of maximum intensity projection of z-stack images acquired by Airyscan imaging was performed using Gwyddion (http://gwyddion.net/).

Data representation and statistical analysis

3D representations of airyscan images were generated with the 3/4D visualization and analysis software Imaris (Oxford Instruments).

Plots were generated using web-based data visualization tools (Shiny apps, https://huygens.science.uva.nl): PlotsOfData[32], PlotTwist, and PlotsOfDifferences. Unless stated otherwise, data is represented as violin plots reflecting the data distribution and the median of the data. Vertical bars indicate for each median the 95% confidence interval determined by bootstrapping.

Statistical analysis was performed using Prism GraphPad software. Unpaired two-tailed t-test with Welch's correction (not assuming equal s.d.) was used to assess significance of experiments done on hypo-osmotic treated cells. One-way analysis of variance-ANOVA Kruskal-Wallis test for multiple comparisons was used to assess significance of experiments done on cells treated with actin drugs. Statistical significance show represents: $^{***}P < 0.001$, $^{****}P < 0.0001$. Experiments represent $N \geq 3$ replicates.

References

1. Zhao, W. *et al*. Nanoscale manipulation of membrane curvature for probing endocytosis in live cells. *Nature Nanotech* **12**, 750–756 (2017).
2. Galic, M. *et al*. External push and internal pull forces recruit curvature-sensing N-BAR domain proteins to the plasma membrane. *Nat Cell Biol* **14**, 874–881 (2012).
3. Vogel, V. & Sheetz, M. Local force and geometry sensing regulate cell functions. *Nat Rev Mol Cell Biol* **7**, 265–275 (2006).
4. Peroz, C., Chauveau, V., Barthel, E. & Søndergård, E. Nanoimprint Lithography on Silica Sol–Gels: A Simple Route to Sequential Patterning. *Advanced Materials* **21**, 555–558 (2009).
5. Gopal, S. *et al*. Porous Silicon Nanoneedles Modulate Endocytosis to Deliver Biological Payloads. *Adv. Mater*. **31**, 1806788 (2019).
6. Shiu, J.-Y., Aires, L., Lin, Z. & Vogel, V. Nanopillar force measurements reveal actin-cap-mediated YAP mechanotransduction. *Nat Cell Biol* **20**, 262–271 (2018).
7. Shin, N.-Y. *et al*. Dynamin and endocytosis are required for the fusion of osteoclasts and myoblasts. *J Cell Biol* **207**, 73–89 (2014).
8. Humphries, A. C. & Way, M. The non-canonical roles of clathrin and actin in pathogen internalization, egress and spread. *Nat Rev Microbiol* **11**, 551–560 (2013).
9. Gauthier, N. C., Masters, T. A. & Sheetz, M. P. Mechanical feedback between membrane tension and dynamics. *Trends in Cell Biology* **22**, 527–535 (2012).
10. Zhang, Q. *et al*. Tailoring the crystal growth of quartz on silicon for patterning epitaxial piezoelectric films. *Nanoscale Adv*. 10.1039.C9NA00388F (2019). doi:10.1039/C9NA00388F
11. Zhang, Q. *et al*. Nanostructure engineering of epitaxial piezoelectric α-quartz thin films on silicon. Preprint at https://arxiv.org/ftp/arxiv/papers/1908/1908.07016
12. Schermelleh, L. *et al*. Super-resolution microscopy demystified. *Nat Cell Biol* **21**, 72–84 (2019).

13. Santybayeva, Z. *et al*. Fabrication of quartz microcylinders by laser interference lithography for angular optical tweezers. *JM3* **15**, 034507 (2016).

14. McMahon, H. T. & Boucrot, E. Molecular mechanism and physiological functions of clathrin-mediated endocytosis. *Nat Rev Mol Cell Biol* **12**, 517–533 (2011).

15. Posor, Y., Eichhorn-Grünig, M. & Haucke, V. Phosphoinositides in endocytosis. *Biochimica et Biophysica Acta (BBA) - Molecular and Cell Biology of Lipids* **1851**, 794–804 (2015).

16. Blanchoin, L., Boujemaa-Paterski, R., Sykes, C. & Plastino, J. Actin Dynamics, Architecture, and Mechanics in Cell Motility. *Physiological Reviews* **94**, 235–263 (2014).

17. Kirchhausen, T., Owen, D. & Harrison, S. C. Molecular Structure, Function, and Dynamics of Clathrin-Mediated Membrane Traffic. *Cold Spring Harb Perspect Biol* **6**, (2014).

18. Parton, R. G. & del Pozo, M. A. Caveolae as plasma membrane sensors, protectors and organizers. *Nat Rev Mol Cell Biol* **14**, 98–112 (2013).

19. Barbieri, E., Di Fiore, P. P. & Sigismund, S. Endocytic control of signaling at the plasma membrane. *Current Opinion in Cell Biology* **39**, 21–27 (2016).

20. Saarikangas, J., Zhao, H. & Lappalainen, P. Regulation of the Actin Cytoskeleton-Plasma Membrane Interplay by Phosphoinositides. *Physiological Reviews* **90**, 259–289 (2010).

21. Ceccato, L. *et al*. PLIF: A rapid, accurate method to detect and quantitatively assess protein-lipid interactions. *Sci. Signal*. **9**, rs2–rs2 (2016).

22. Colom, A. *et al*. A fluorescent membrane tension probe. *Nature Chem* **10**, 1118–1125 (2018).

23. Pietuch, A., Brückner, B. R. & Janshoff, A. Membrane tension homeostasis of epithelial cells through surface area regulation in response to osmotic stress. *Biochimica et Biophysica Acta (BBA) - Molecular Cell Research* **1833**, 712–722 (2013).

24. Baschieri, F. *et al*. Frustrated endocytosis controls contractility-independent mechanotransduction at clathrin-coated structures. *Nat Commun* **9**, 3825 (2018).

25. Saffarian, S., Cocucci, E. & Kirchhausen, T. Distinct Dynamics of Endocytic Clathrin-Coated Pits and Coated Plaques. *PLoS Biol* **7**, e1000191 (2009).
26. de Boor, J., Geyer, N., Wittemann, J. V., Gösele, U. & Schmidt, V. Sub-100 nm silicon nanowires by laser interference lithography and metal-assisted etching. *Nanotechnology* **21**, 095302 (2010).
27. Cocucci, E., Gaudin, R. & Kirchhausen, T. Dynamin recruitment and membrane scission at the neck of a clathrin-coated pit. *MBoC* **25**, 3595–3609 (2014).
28. Aguet, F. *et al*. Membrane dynamics of dividing cells imaged by lattice light-sheet microscopy. *MBoC* **27**, 3418–3435 (2016).
29. Sinha, B. *et al*. Cells Respond to Mechanical Stress by Rapid Disassembly of Caveolae. *Cell* **144**, 402–413 (2011).
30. Picas, L. *et al*. BIN1/M-Amphiphysin2 induces clustering of phosphoinositides to recruit its downstream partner dynamin. *Nat Commun* **5**, 5647 (2014).
31. Schneider, C. A., Rasband, W. S. & Eliceiri, K. W. NIH Image to ImageJ: 25 years of image analysis. *Nat Methods* **9**, 671–675 (2012).
32. Postma, M. & Goedhart, J. PlotsOfData—A web app for visualizing data together with their summaries. *PLoS Biol* **17**, e3000202 (2019).

Acknowledgements

The authors thank D. Montero for performing the FEGSEM images. B. Charlot and R. Desgarceaux from IES for providing the silicon mold. C. Cazevielle (MRI-COMET, Montpellier) for assistance with SEM images. C. Favard, D. Muriaux, and N. Sauvonnet for scientific discussions. We acknowledge the imaging facility MRI, member of the national infrastructure France-BioImaging infrastructure supported by the French National Research Agency (ANR-10-INBS-04, «Investments for the future»). The authors are grateful to A. Roux for the support provide to this work. L.P. acknowledges the ATIP-Avenir program for financial support. A.C-G. acknowledges the financial support from the European Research Council

(ERC) under the European Union's Horizon 2020 research and innovation program (No.803004) and the French Agence Nationale de la Recherche (ANR), project Q-NOSS ANR ANR-16-CE09-0006-01; The FEGSEM instrumentation was facilitated by the Institut des Matériaux de Paris Centre (IMPC FR2482) and was funded by Sorbonne Université, CNRS and by the C'Nano projects of the Région Ile-de-France.

Author contributions

T.S., D.S, R.R., A.C-D. performed experiments and analyzed results. F.E-A. and J.V. generated the PI-probes. S.R. designed the semi-automatic analysis of images. R.G. generated the genome-edited SUM-159 cell lines. M.M. and S.M. synthetized the FliptR probe. A.C-G. and L.P. supervised the study, designed experiments and wrote the manuscript. All authors contributed to final version of the paper.

Supplementary information

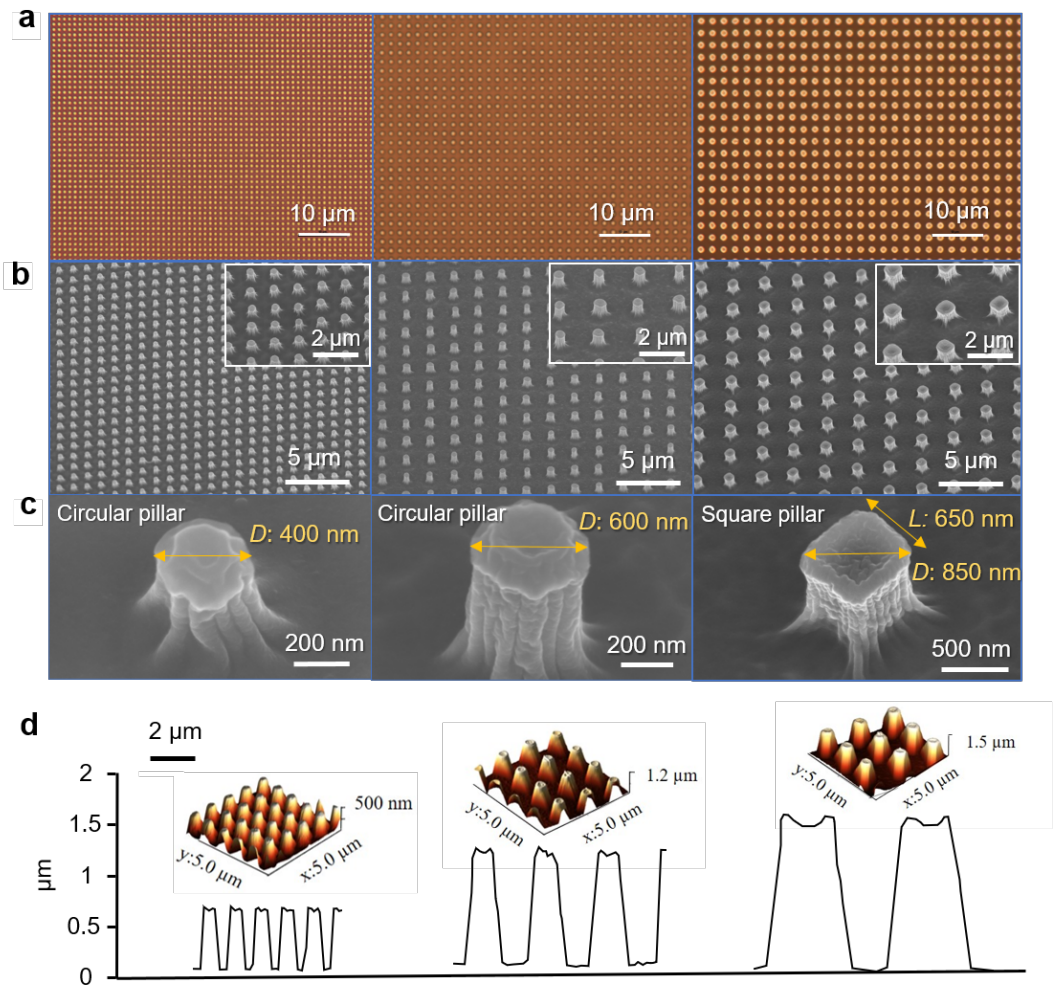

Supplementary Figure 1. Characterization of 1D vertical SiO_2 nanopillars used in this work. a, Optical images of Si(100) masters used along this work obtained by using LIL lithography. **b**, FEG-SEM images of printed silica nano-pillars with controlled diameter i.e. 400 and 600 nm of diameter for the circular pillars and 800 nm of diagonal for squared nano pillars. **c**, FEG-SEM images at higher magnification of pillars showing the different dimensions. **d**, 3D AFM images showing silica nanostructured films prepared by NIL lithography in b. Below you can distinguish the profile analysis of the AFM image in b, revealing a perfect transfer of the different motives.

Supplementary table 1. Dimensions of the 1D SiO_2 vertical nanopillars used in this study established from FEG-SEM and AFM images.

Pillar dimension (SEM analysis)	Pillar shape (SEM analysis)	Pillar height (AFM analysis)	Motif periodicity (SEM analysis)
Diameter = 400 nm	Circular	650 nm	1000 nm
Diameter = 600 nm	Circular	1200 nm	1700 nm
Diagonal = 850 nm **Side length = 600 nm**	Square	1500 nm	2400 nm

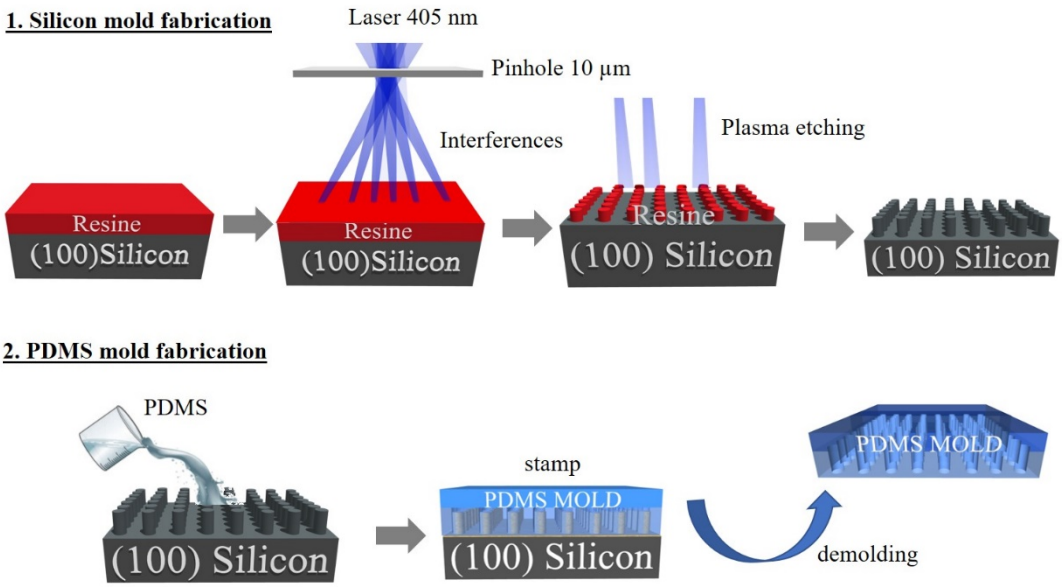

Supplementary Figure 2. Schematics summarizing the key steps that were applied to produce the PDMS mold.

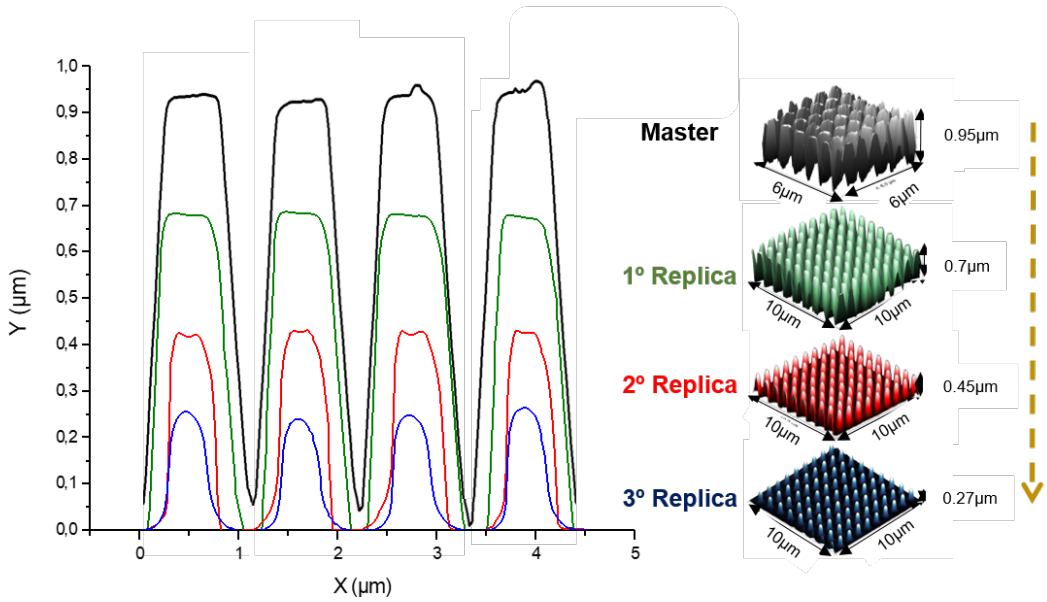

Supplementary Figure 3. Control of vertical SiO_2 nanocolumn dimensions by a multiple replication process of the original silicon master. Notice that after applying this method the silica nanopillar reduces their dimension

of 40% each NIL process approximately, which correspond around 200 nm less in height from the original silicon master (black line).

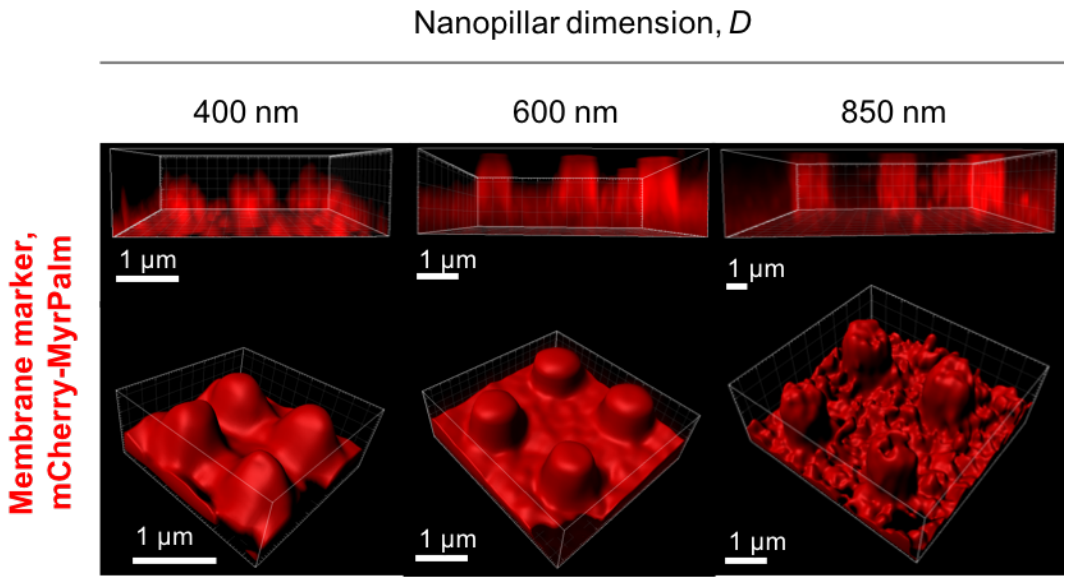

Supplementary Figure 4. Characterization of the plasma membrane deformation imposed by the underlying vertical SiO_2 nanocolumns. 3D reconstruction of a cross-section (*upper panel*) top view (*bottom panel*) of HeLa cells seeded on vertical nanopillars of $D \sim 400$ nm, $D \sim 600$ nm, and $D \sim 850$ nm and stained with the cell plasma membrane marker mcherry-MyrPalm. Scale bar, 1 µm.

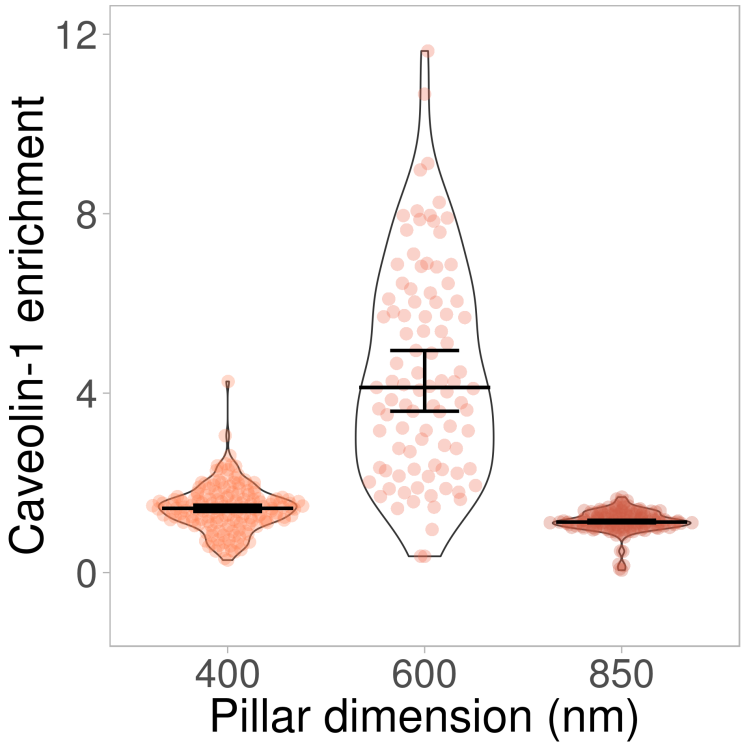

Supplementary Figure 5. Quantification of the enrichment of the endocytic protein caveolin-1 at nanopillar locations. Estimation of the enrichment, *E*, of caveolin-1 from immunostained HeLa cells seeded on nanopillars of *D* ~ 400 nm, *D* ~ 600 nm, and *D* ~ 850 nm. Data is shown as violin plots reflecting the data distribution and the median of the data. Vertical bar indicates for each median the 95% confidence interval determined by bootstrapping. The number of data points that are represented per condition is: *n*=169, *n*=95, *n*=145, for *D* ~ 400 nm, *D* ~ 600 nm, and *D* ~ 850 nm, respectively.

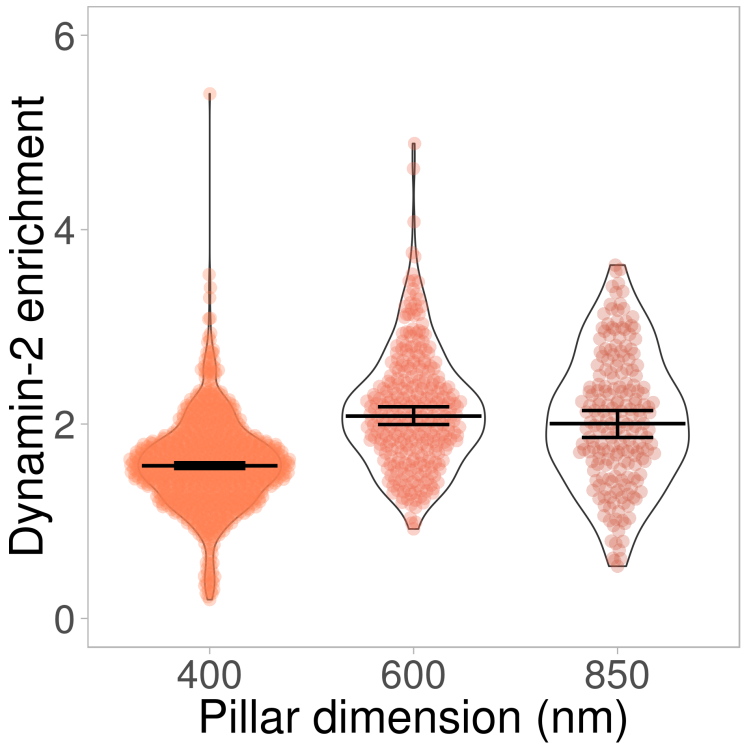

Supplementary Figure 6. Quantification of the enrichment of the endocytic protein dynamin-2 at nanopillar locations. Estimation of the enrichment, *E*, of dynamin-2 from genome edited SUM-159 Dynamin2-EGFP cells seeded on nanopillars of *D* ~ 400 nm, *D* ~ 600 nm, and *D* ~ 850 nm. Data is shown as violin plots reflecting the data distribution and the median of the data. Vertical bar indicates for each median the 95% confidence interval determined by bootstrapping. The number of data points that are represented per condition is: *n*=889, *n*=311, *n*=204, for *D* ~ 400 nm, *D* ~ 600 nm, and *D* ~ 850 nm, respectively.

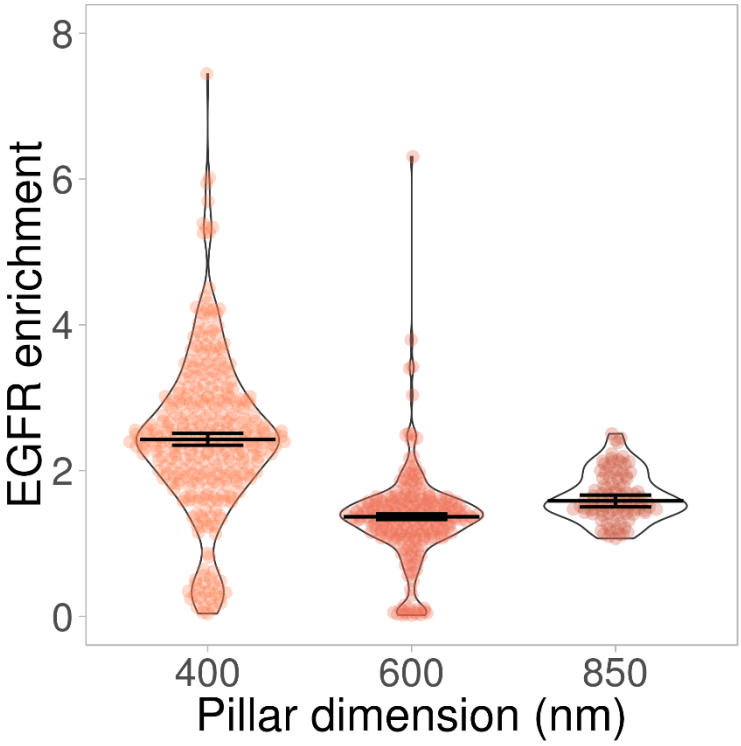

Supplementary Figure 7. Quantification of the enrichment of the EGFR at nanopillar locations. Estimation of the enrichment, *E*, of the EGFR on HeLa cells seeded on nanopillars of *D* ~ 400 nm, *D* ~ 600 nm, and *D* ~ 850 nm that were transiently transfected with EGFR-GFP. Data is shown as violin plots reflecting the data distribution and the median of the data. Vertical bar indicates for each median the 95% confidence interval determined by bootstrapping. The number of data points that are represented per condition is: *n*=332, *n*=231, *n*=96, for *D* ~ 400 nm, *D* ~ 600 nm, and *D* ~ 850 nm, respectively.

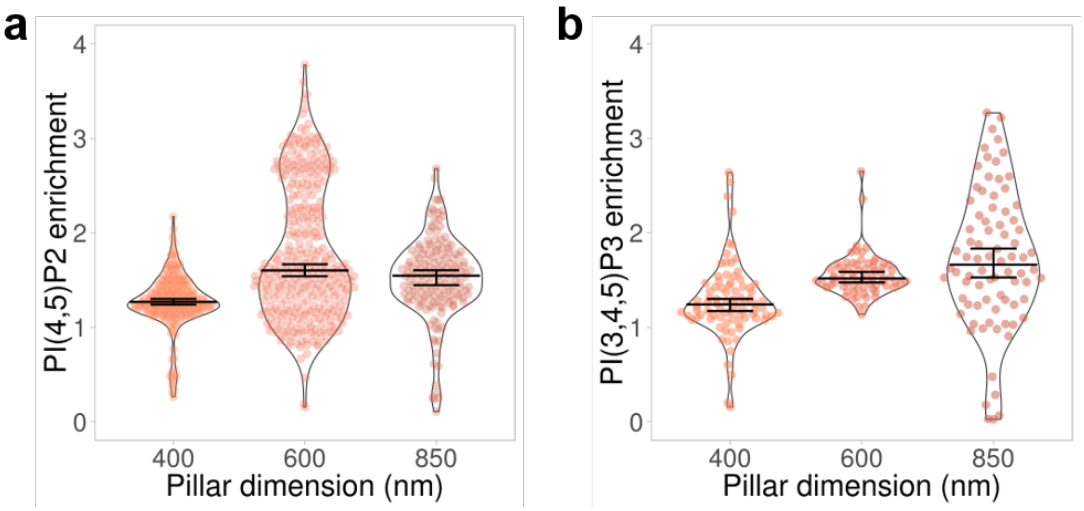

Supplementary Figure 8. Quantification of the enrichment of the plasma membrane phosphoinositides PI(4,5)P_2 and PI(3,4,5)P_3 at nanopillar locations. a-b, Estimation of the enrichment, *E*, of PI(4,5)P_2 (**a**) and

PI(3,4,5)P_3 (**b**) on HeLa cells seeded on nanopillars of $D \sim 400$ nm, $D \sim 600$ nm, and $D \sim 850$ nm. Data is shown as violin plots reflecting the data distribution and the median of the data. Vertical bar indicates for each median the 95% confidence interval determined by bootstrapping. The number of data points that are represented per condition is n=218, n=345, n=161 for PI(4,5)P_2 and n=82, n=70, n=80 for PI(3,4,5)P_3, for $D \sim 400$ nm, $D \sim 600$ nm, and $D \sim 850$ nm, respectively.

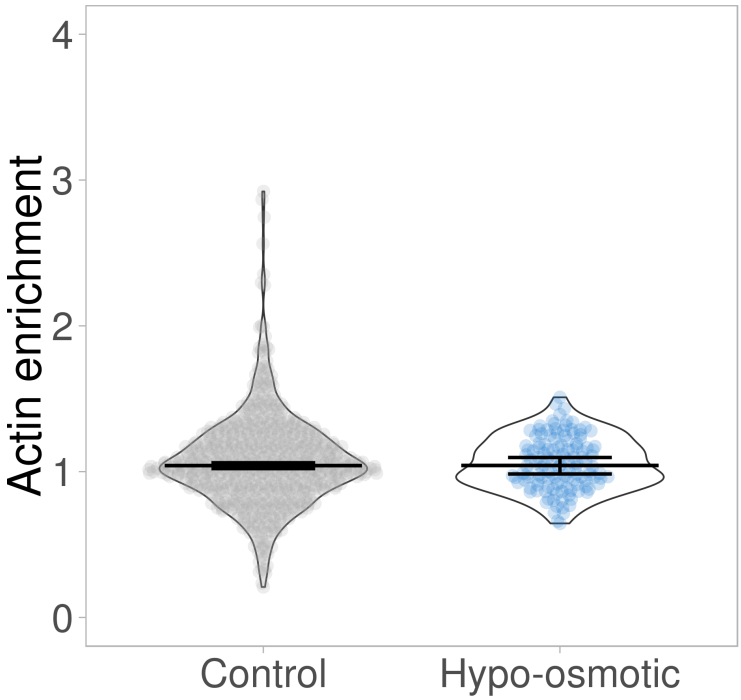

Supplementary Figure 9. Estimation of the enrichment, E, of actin on nanopillar locations from stained HeLa cells seeded on nanopillars of $D \sim 850$ nm under hypo-osmotic shock ($\Pi < 300$ mOsm) (*in blue*). Comparison with the non-treated condition, i.e. isotonic condition, is shown in grey. Data is shown as violin plots reflecting the data distribution and the median of the data. Vertical bar indicates for each median the 95% confidence interval determined by bootstrapping. The number of data points that are represented per condition is n=649 and n=129 for the non-treated and under osmotic swelling, respectively.